Luminescence kinetics in Ce-doped $Tb_xGd_{3-x}Al_5O_{12}$ garnet with various terbium content

Saulius Nargelas[1], Arnoldas Solovjovas[1], Gabija Soltanaitė[1], Žydrūnas Podlipskas[1], Yuriy Zorenko[2], Vitaliy Gorbenko[2], Etiennette Auffray[3], Gintautas Tamulaitis[1]

[1] Vilnius University, Institute of Photonics and Nanotechnology, Sauletekio 3, LT-10257, Vilnius, Lithuania
[2]Department of Physics, Kazimierz Wielki University in Bydgoszcz, Powsta´nców Wielkopolskich Str., 2, 85-090 Bydgoszcz, Poland
[3]European Organization for Nuclear Research (CERN), Geneva, Switzerland

Highlights:

Homogeneous Tb-containing garnet film scintillators are grown by liquid phase epitax
Time-resolved photo- and cathodo-luminescence spectroscopy exploited
Acceleration of luminescence decay by introduction of Tb demonstrated
Tb^{3+} ions provide prompt photons in subnanosecond domain
Electron transfer from activator Ce^{3+} to nearest Tb^{3+} is faster than that vice versa

Keywords

Scintillator, Terbium Gadolinium aluminum Garnet, Excitation transfer, Ce activator, Luminescence, Cathodoluminescence

Abstract

In view of the current demand of fast scintillators for ionizing radiation detectors for high energy physics experiments and medical imaging, the excitation transfer between host crystal and activator ions in activated scintillators is increasingly important phenomenon. The current study is focused on the excitation transfer in Ce-doped terbium gadolinium aluminum garnets with different ratios of Tb and Gd ions in the host lattice. Scanning electron microscopy and cathodoluminescence images show that the liquid phase epitaxy (LPE) using $PbO\text{-}B_2O_3$ flux ensure the fabrication of thin single crystalline films of such scintillators of high structural homogeneity. Time-resolved photo- and cathodo-luminescence spectroscopy of the films revealed that the electron transfer from activator ion Ce^{3+} to the nearest lattice-building ions Tb^{3+} is faster than that *vice versa*. The acceleration of the decay of Ce^{3+} luminescence by introduction of Tb is demonstrated, whereas the Tb^{3+} ions emit prompt photons in subnanosecond domain but this emission is strongly quenched by nonradiative recombination. We show that the excitation transfer from Ce^{3+} to the closest Tb^{3+} is the dominant mechanism accelerating the emission decay of $Tb_xGd_{3-x}Al_5O_{12}$:Ce operating as a scintillator.

1. Introduction

Cerium-doped yttrium aluminum garnet (YAG:Ce) is currently the main phosphor in all conventional industrial white light-emitting diodes (LEDs). YAG:Ce is also attractive as a scintillator material [1]. However, in contrast to the direct absorption of the blue emission of InGaN chips by the emitting Ce^{3+} ions in white LEDs, the excitation after the interaction of scintillator with high-energy photons has to be transferred to the emitting Ce^{3+} centers. This transfer is affected by electron traps delaying the luminescence response and channeling a part of the excitation to the centers of nonradiative recombination. These electron traps might be buried in the conduction band by the substitution of a part of Al ions by Ga ions that results in a downshift of the bottom of the conduction band [2]. However, the downshift decreases the energy barrier for thermal depopulation of the Ce^{3+} emitting level and results in luminescence quenching. The depopulation barrier can be increased by substitution of Y by Gd in gallium gadolinium aluminum garnet (GAGG:Ce) [3,4,5] exhibiting a record-high light yield of 58 000 ph/MeV in $Gd_3Al_{2.3}Ga_{2.7}O_{12}$:Ce [6] and close values achieved in many other laboratories and even at industrial level.

The aliovalent codoping [7,8] and the carrier localization due to composition fluctuations in a multicomponent garnet lattice [9,10] are shown to be beneficial for the further improvement of the GAGG:Ce scintillators. Moreover, the single crystals of Ga-containing garnets have to be grown from high-temperature melt requiring expensive iridium crucibles. In addition, in GAGG:Ce crystals grown in such conditions contain neutral antisite defects Gd_{Ga} , whereas, evaporative GaO oxide escapes from open crucible, and vacancies of oxygen V_O and V_{Ga} are created. All these defects might participate in the process of energy transfer from the GAGG host to the Ce^{3+} ions as recombination and trapping centers, thus, leading to the deterioration of scintillation properties of GAGG:Ce crystals.

Another alternative to mitigate the deteriorating influence of traps in garnet-type hosts for Ce-based scintillators is growing the garnets at low-temperature from the melt-solution using liquid phase epitaxy (LPE) method. Generally, the most probable type of traps in garnets is antisite defects. It is theoretically shown that they have the lowest formation energy among the intrinsic defects in YAG and other garnets [11], and their high density is experimentally demonstrated in YAG single crystals that have to be grown at high temperatures (1800–1900 ^{0}C) [12]. However, the concentration of such defects is shown to be substantially lower in thin single crystalline films

(SCF) of garnet compounds grown using LPE method at lower temperatures (850–1100 ^{0}C) [13]. This approach is exploited in the current paper.

In this, we are also exploiting the flexibility of multicomponent garnets to accommodate various ions without significant deterioration of the garnet lattice. Our work was aimed at studying the influence of the introduction of terbium on the emission properties of Ce-doped Ga-free gadolinium aluminum garnet with a fraction of Gd substituted by Tb. We focus on the study of energy transfer between the matrix-building ions and the activator ion Ce^{3+}.

It is demonstrated that the energy transfer to the emitting Ce^{3+} via the Gd subsystem in a garnet-type matrix is delayed and deteriorates the timing properties of Gd-containing garnet scintillators [14]. Meanwhile, fast excitation transfer via the Tb subsystem in high-Tb-content garnets was observed in $(Lu,Tb)_3Al_5O_{12}$ [15] and $Gd_{3-x}Tb_xAl_5O_{12}$ [16]. Moreover, an efficient excitation transfer from the $^5D_4$ level of Tb^{3+} to the emitting $5d_1$ level of Ce^{3+} is demonstrated to be efficient and bidirectional [17,18,19]. An energy diagram explaining the excitation transfer between Gd^{3+}, Tb^{3+} and Ce^{3+} is suggested [20]. Therefore, the decay acceleration for the emission of activator ion Ce^{3+} might be expected due to i) fast excitation transfer through the garnet matrix enhanced by the transfer via the Tb sublattice and/or ii) fast depopulation of Ce^{3+} centers to Tb^{3+}. These issues are addressed in the current paper.

To reveal the influence of Tb on the emission intensity and decay rate, three thin layers of Ce-doped $Tb_xGd_{3-x}Al_5O_{12}$ with Tb content x = 0.5, 1.3, and 1.5 were grown and investigated. Steady-state and time-resolved photoluminescence (PL) and cathodoluminescence (CL) spectroscopies were used to exploit the excitation resonantly to certain energy levels of Ce^{3+}, Tb^{3+}, and Gd^{3+} in PL experiments and the generation of high-energy nonequilibrium carriers by accelerated electrons in CL experiments.

2. Experimental

2.1. Samples

Three samples of Ce-doped gadolinium terbium aluminum garnet with various ratios between Tb and Gd contents have been fabricated for the study: $Tb_{0.5}Gd_{2.5}Al_5O_{12}$:Ce, $Tb_{1.3}Gd_{1.7}Al_5O_{12}$:Ce, and $Tb_{1.5}Gd_{1.5}Al_5O_{12}$:Ce. The thicknesses of all three layers were similar: 9, 10, and 13 μm, respectively. The thin layers were grown on nominally undoped $Y_3Al_5O_{12}$ substrates using the

liquid phase epitaxy (LPE) technique in platinum crucible from a supercooled melt solution based on PbO-B_2O_3 flux. Oxides Tb_4O_7, Gd_2O_3, Al_2O_3, and CeO_2 of 4N purity were used as the garnet-forming constituents. The growth conditions were as described in detail in [21,22].

2.2. Measurement techniques

In photoluminescence (PL) experiments, Yb:KGW laser *Pharos* (*Light Conversion*) emitting 170 fs pulses at a wavelength of 1030 nm was used as an excitation source. Modules for harmonics generation and optical parametric amplifier *Orpheus* (*Light Conversion*) were exploited to tune the excitation wavelength stepwise and continuously. PL spectroscopy was carried out using an *Andor* 328-mm-focal-length spectrograph *Kymera 328i*, equipped with a *Hamamatsu* UV-VIS BT-CCD camera for time-integrated PL measurements and with a *Hamamatsu* UV-VIS streak camera C10910-01 in time-resolved measurements ensuring 30 ps resolution. The decay was analyzed by fitting the measured PL kinetics with a multiexponential function.

The PL quantum efficiency (QE) was estimated at pulsed excitation tuned at specific wavelength in resonance to targeted optical transitions by the method described in [23] and using the required three spectra measured in different configurations in a *Gigahertz Optik* 6-inch-diameter integrating sphere coated with $BaSO_4$.

Attolight spectrometric system *Chronos* was used in cathodoluminescence (CL) spectroscopy with time resolution and for spatial mapping. Short pulses of electrons accelerated at a voltage of 10 kV were generated by triggering the electron gun with a *NKT Photonics* picosecond laser *aeroPULSE PS* operating at a pulse repetition rate of 2 MHz. The luminescence was dispersed by a *Horiba* spectrometer *iHR 320* and recorded using an *Andor* Charge-Coupled Device (CCD) camera *Newton 920* for mapping or a *Hamamatsu* streak camera *C10910* for measuring CL time evolution with overall time resolution of ~100 ps. To reconstruct the luminescence decay in a wide time range, the results of measurements in multiple temporal windows were compiled. The surface morphology was studied in scanning electron microscopy (SEM) mode of the *Chronos* system at CW operation.

All the measurements are performed at room temperature.

3. Results

3.1. Surface morphology

SEM images of typical areas on the surface of the three samples under study are presented in Fig. 1a,b,c. Introduction of more Tb facilitates the formation of laminaria-shaped structures, though the surface roughness is quite small in all the samples. In addition, a few small pits with a diameter of ~10 nm can be spotted in the SEM images. The surface morphology correlates with the spatial distribution of the luminescence intensity scanned in cathodoluminescence experiments (see Fig. 1d,e,f). The spatial variations of luminescence intensity might be affected either by changes in local emission intensity or in light extraction due to surface morphology. However, the inhomogeneities observed in SEM and CL images are substantially smaller than the diameter of the excitation spot in photoluminescence experiments. Thus, a spatially averaged intensity was detected in our PL spectroscopy experiments.

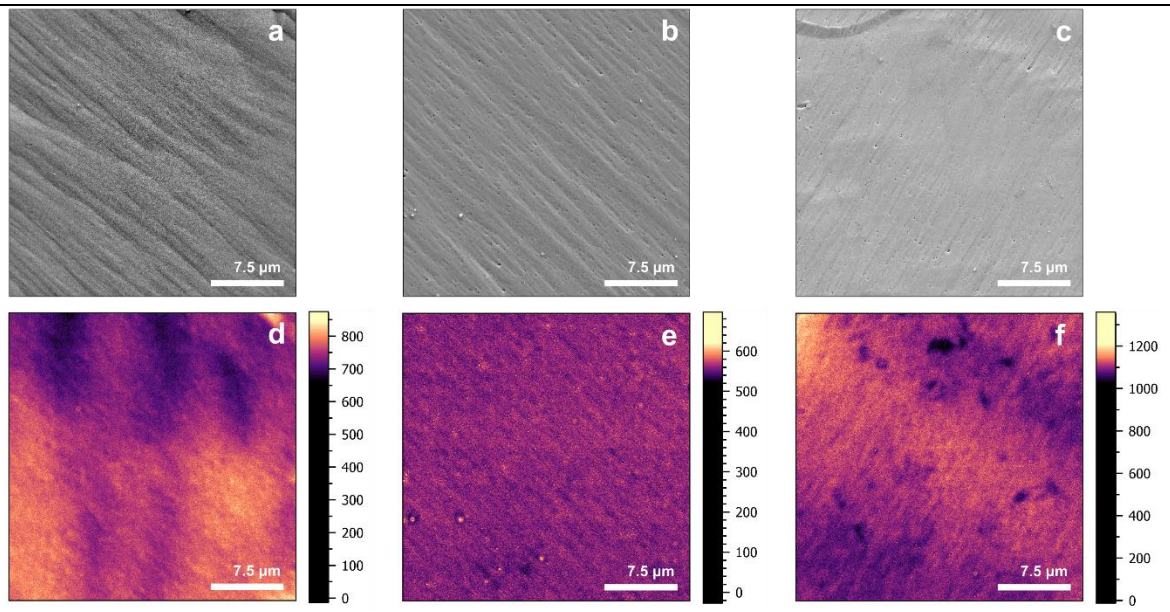

Fig. 1. Scanning electron microscopy (SEM) (a, b, c) and cathodoluminescence (CL) intensity (d, e, f) images of $Tb_xGd_{3-x}Al_5O_{12}$ layers with x = 1.5 (a, d), 1.3 (b, e), and 0.5 (c, f).

3.2. Optical absorption

Absorption spectra of the three samples with various ratios of Tb and Gd content are presented in Fig. 2. The strong absorption bands peaked at 275 nm and 220 nm are truncated due to the low level of the light transmitted through the layer. The optical transitions identified as responsible for the absorption in this spectral region are indicated above the corresponding peaks. The selection of the excitation wavelengths was based on these results. The wavelength of 464 nm was selected

to excite selectively the Ce^{3+} ion resonantly to the lowest excited level $5d^1$. Higher absorption bands are partially overlapped. The second selected excitation wavelength of 331 nm corresponds to the peak of the band due to absorption to the Ce^{3+} level $5d^2$. However, Tb^{3+} ions might also partially absorb at this wavelength due to forbidden high-spin $4f^8 \rightarrow 4f^7 5d^1$ electron transition resulting in the absorption band peaked at 322 nm [24]. The third excitation wavelength of 275 nm was selected at the dominant absorption band of Tb^{3+} due to low-spin $4f^8 \rightarrow 4f^7 5d^1$ electron transition. The excitation of Gd^{3+} ion to its excited state ^6I_J is also expected at this wavelength [25]. This strong absorption band presented in Fig.2 is truncated due to a very weak light detected at the band. Moreover, certain sample-dependent contribution of scattered light and reflection conditions might have a significant influence on the signal detected. Thus, substantially thinner layers would be required to compare the absorption band in different samples.

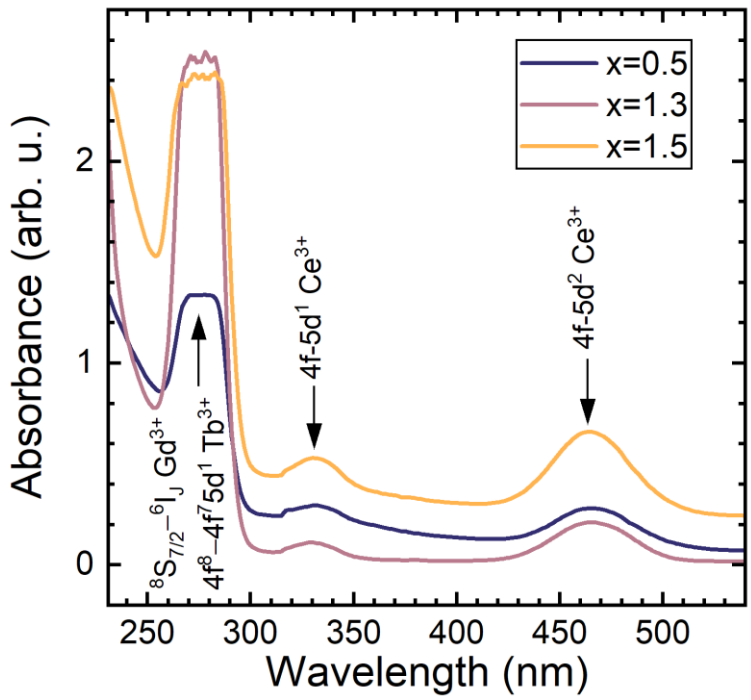

Fig. 2. Absorbance spectra of Ce-doped garnets containing Gd and Tb cations at different ratios (indicated).

3.3. Photoluminescence spectra and time evolution

To follow the expected excitation transfer, photoluminescence properties were studied under pulsed excitation at three wavelength, 464 nm, 331 nm, and 275 nm, selected to resonantly excite Ce^{3+} ions to the lowest excited levels $5d_1$ and $5d_2$, and Tb^{3+} to ^6I_J, respectively.

The wavelength 464 nm corresponds to the optical transition from the lowest ground state to the lowest excited state $5d_1$ of the activator ion Ce^{3+}. No excitation of lattice-building ions in the garnets under study is expected at this wavelength. The emission spectra of all three samples studied [see Fig. 3(a)] consist of two strongly overlapping emission bands due to Ce^{3+} optical transitions from $5d_1$ to the split ground states $^2F_{5/2}$ and $^2F_{7/2}$. No sharp emission lines typical of Tb^{3+} and Gd^{3+} are observed, evidencing the dominance of Ce^{3+} emission at this selective excitation of the activator ion. Meanwhile, the PL decay kinetics (see Fig.3b) is different from that expected for an isolated Ce^{3+} ion in a garnet lattice (typically a single-exponential decay with a time constant of ~50 ns [26]). The PL decay in all three samples studied has three components: fast initial decay, intermediate decay at the rate typical of the decay of an isolated Ce^{3+} ion, and a slow decay component. The contributions of the first and third components increase with increasing Tb content in the garnet structure. This increase is especially pronounced in the sample with the highest Tb content of $x = 1.5$.

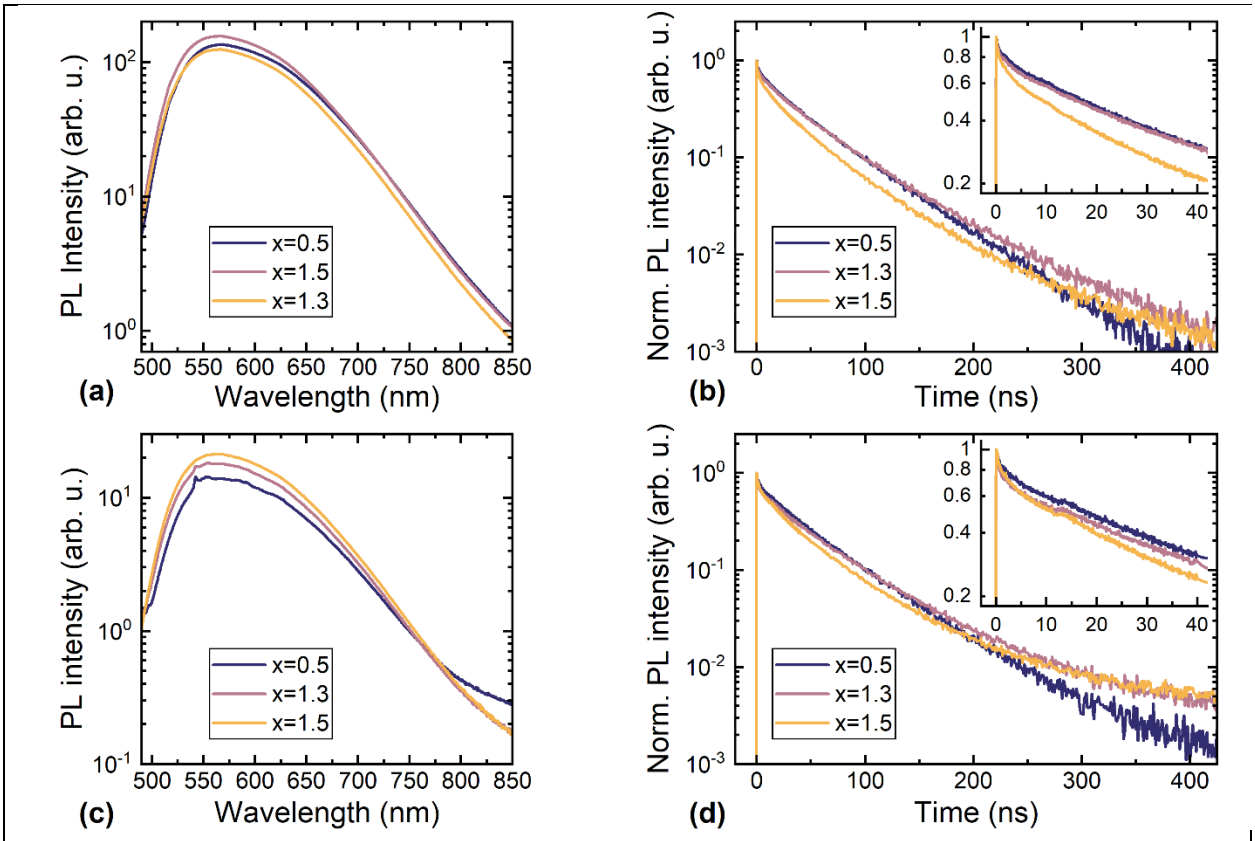

Fig. 3. Time-integrated photoluminescence spectra (a, c) and decay kinetics of spectrally-integrated intensity (b, d) for $Tb_xGd_{3-x}Al_5O_{12}$:Ce with varying Tb content x (indicated) under

464 nm (a, b) and 331 nm (c, d) excitation. The initial part of the intensity decay are extended in the insets.

The PL spectra and decay kinetics at excitation of Ce^{3+} ion resonantly to its second excited state $5d_2$ (at 331 nm) are presented in Fig. 3(c,d). In addition to the broad bands due to Ce^{3+} emission, the spectra exhibit also certain sharp lines evidencing the contribution of Tb^{3+} emission. The PL decay kinetics have three components, similarly to the case of excitation to $5d_1$ of Ce^{3+}.

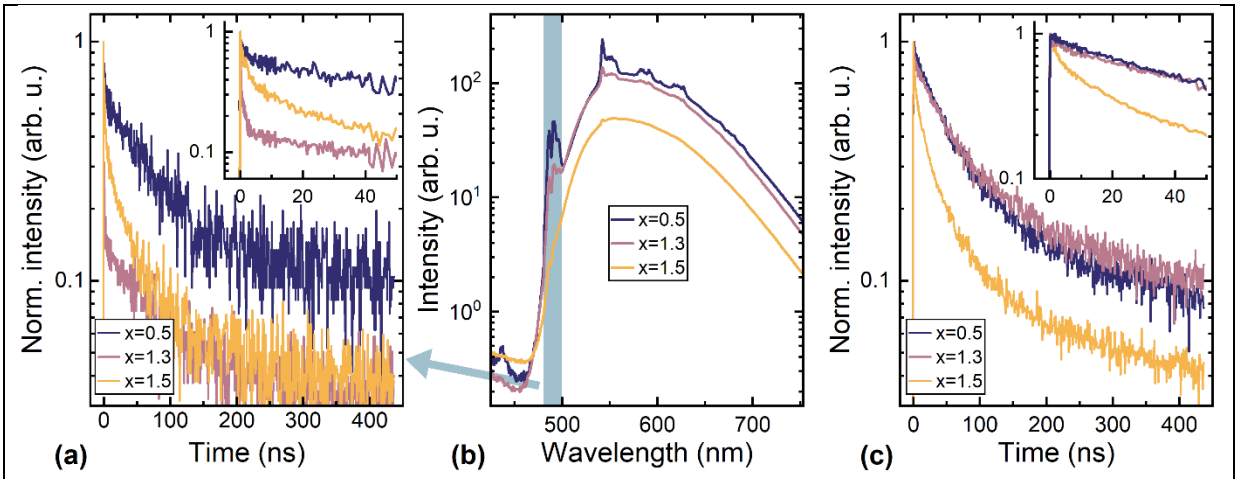

Fig. 4. Time-integrated spectra (b) and decay of spectrally-integrated photoluminescence intensity in the range dominated by emission of Tb^{3+} (a) and Ce^{3+} (c) in $Tb_xGd_{3-x}Al_5O_{12}$:Ce with different Tb content *x* (indicated) after excitation at 275 nm. The initial parts of the intensity decay are extended in the insets.

The PL properties at the excitation wavelength of 275 nm corresponding to the resonant excitation of Gd^{3+} ion to its excited state ^6I_J and Tb^{3+} ion to its excited state $4f^75d^1$ are illustrated in Fig. 4. The PL spectra at this excitation have contributions of two strongly overlapping broad bands due to Ce^{3+} emission and narrow structured bands peaked approximately at 485, 542, 585, and 620 nm. These lines are caused by the emission of Tb^{3+} ions via optical transitions from $^5D_4$ to $^7F_{6,5,4,3}$, as observed in $Tb_xGd_{3-x}Al_5O_{12}$:Ce [27] and for Tb^{3+} emission in other hosts [28,29]. It is worth noting that the contribution of the narrow bands to the total PL spectrum decreases with increasing Tb content and nearly vanishes at $x = 1.5$.

The decay of PL spectrally integrated in the range from 450 to 500 nm, where the Tb^{3+} emission ($^5D_4 \rightarrow {}^7F_6$) is most pronounced, is presented in Fig. 4(a), whereas the decay of predominantly Ce^{3+}emission, spectrally integrated within the entire broad band, is presented in Fig. 4(c).

3.4. Luminescence quantum efficiency

The luminescence quantum efficiency (QE) was measured at two excitation wavelengths: 464 nm and 331 nm corresponding to Ce^{3+} optical transitions from 4f to $5d_1$ and $5d_2$, respectively. The luminescence intensity at resonant excitation of Gd^{3+} was too weak for the QE to be properly estimated. The results are presented in Table 1. The samples studied had thin films on both sides of the substrates. The QE measurements have been carried out for both sides of the samples, and the results coincided within the experimental error of approximately 10%. The estimated QE values listed in Table 1 might be slightly reduced due to the light absorption in the nominally transparent substrate possibly containing a low density of absorption centers. However, the substrate influence on QE, if any, should be similar for all samples studied and impose no substantial corruption of general trends as the Tb content increases. The QE at 464 nm excitation corresponding to the initial population of only Ce^{3+} is similar in layers with a low Tb content, but decreases by more than 30% in the sample with equal contents of Gd and Tb. The QE under excitation at 331 nm, resulting in the initial excitation of both Ce^{3+} and Tb^{3+}, is substantially smaller than that at 464 nm excitation.

Table 1. Quantum efficiency of $Tb_xGd_{3-x}Al_5O_{12}$:Ce with different ratios of Tb to Gd contents for excitation at 464 nm and 331 nm corresponding to Ce^{3+} optical transitions from 4f to $5d_1$ and $5d_2$, respectively.

	Quantum yield, %	
Excitation at	464nm	331nm
$Tb_{0.5}Gd_{2.5}Al_5O_{12}$:Ce	29	4
$Tb_{1.3}Gd_{1.7}Al_5O_{12}$:Ce	30	13

$Tb_{1.5}Gd_{1.5}Al_5O_{12}$:Ce	18	6

3.5. Time-resolved cathodoluminescence

The cathodoluminescence (CL) spectra measured under CW excitation and spatially integrated over the scanned area of 30x30 μm^2 are presented in Fig. 5(a). They are dominated by Ce^{3+} emission resulting in two strongly overlapping bands. In addition, narrow lines of substantially smaller intensity can be traced at ~485 nm and ~542 nm due to Tb^{3+} transitions $^5D_4 \rightarrow {}^7F_6$ and $^5D_4 \rightarrow {}^7F_6$, respectively, as in PL spectra, and in the vicinity of 400 nm, those caused by transitions $^5D_3 \rightarrow {}^7F_{6,5,4}$ [30].

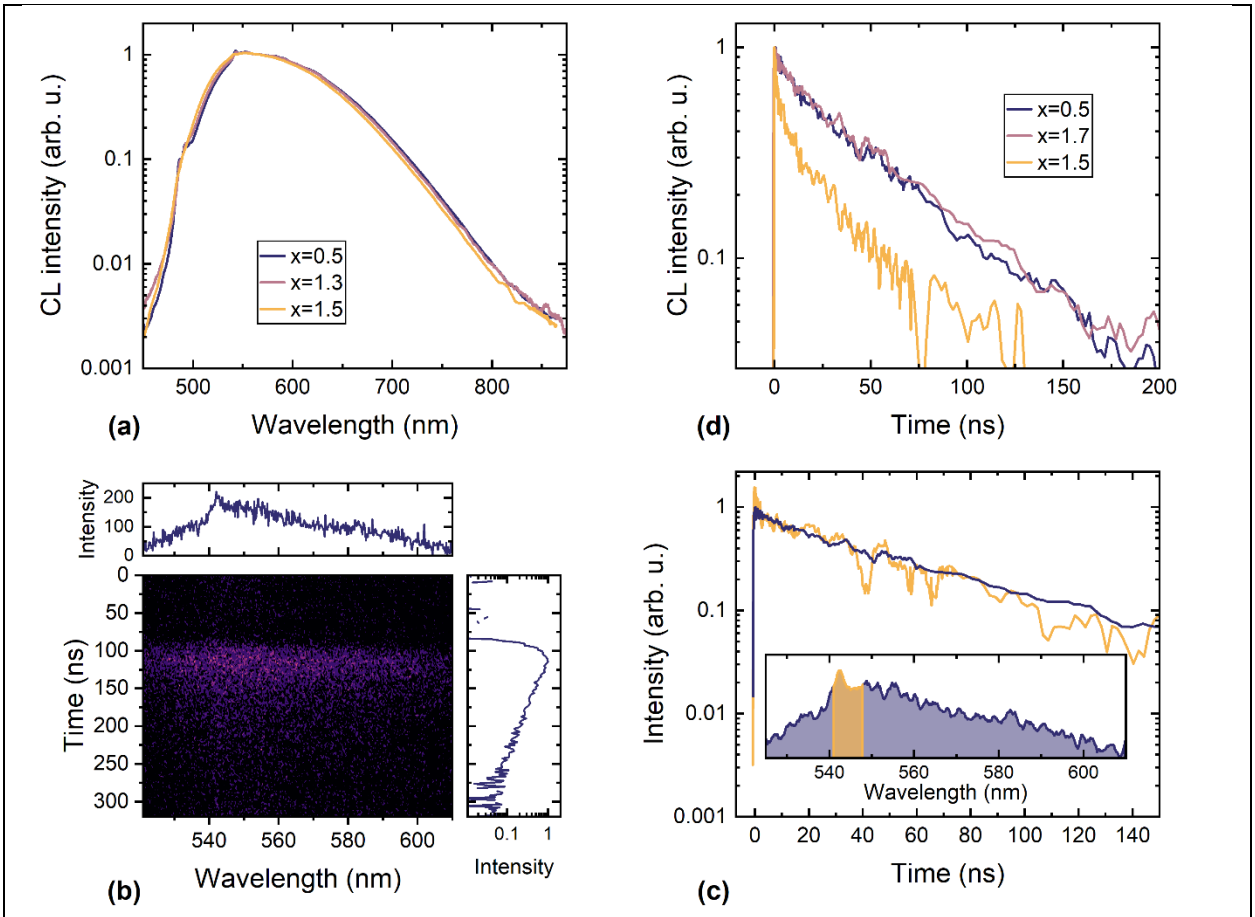

Fig. 5. (a) Normalized spatially-integrated cathodoluminescence spectra of samples with Tb content x=0.5, 1.3, and 1.5 (indicated). (b) Streak-camera image of cathodoluminescence in $Tb_{0.5}Gd_{2.5}Al_5O_{12}$:Ce with time-integrated spectrum (above) and spectrally-integrated intensity kinetics (beside) extracted from the image. (c) Intensity decay transients of cathodoluminescence due to emission of Ce^{3+} (A) and Tb^{3+} (B). The corresponding spectral ranges are indicated in the inset. (d) Decay kinetics of cathodoluminescence in $Tb_xGd_{3-x}Al_5O_{12}$:Ce with different Tb content *x* (indicated).

A typical streak-camera image of CL in $Gd_{2.5}Tb_{0.5}Al_5O_{12}$:Ce is presented in Fig. 5(b). The spectrum is dominated by Ce^{3+} emission and contains a narrow band due to Tb^{3+} emission peaked at 543 nm.

The kinetics of Ce^{3+} and Tb^{3+} CL are compared in Fig. 5(c). The intensities presented are spectrally integrated within the ranges indicated in the inset of Fig. 5(c). The decay transients are shifted vertically to match the part of slow decay. Though the intensity in spectral range B has emission contributions of both Ce^{3+} and Tb^{3+}, the transients evidence that the Tb^{3+} emission has a fast decay component, as the PL transients have.

The fast CL decay component is present also in the transients of CL intensity integrated throughout the entire spectrum (see Fig. 5(d)). This component is best pronounced in the sample with the highest Tb content (x = 1.5).

4. Discussion

SEM and CL intensity maps evidence quite high homogeneity of the layers with Gd content higher than that of Tb. The third sample with equal contents of Gd and Tb in the host lattice has dark spots of 10 nm in diameter. Otherwise, the surface morphology and the distribution of CL intensity are similar to those in the layers with smaller Tb content.

Our study of PL kinetics shows that even at the selective excitation of activator ions Ce^{3+} to their lowest excited state $5d_1$ serving as the emitting level, the luminescence initially proceeds at a rate faster than the rate for individual Ce^{3+} ions in garnet host. This acceleration process saturates within the first tens of nanoseconds after excitation, and the further decay proceeds at the rate typical of the individual Ce^{3+} ions (the PL intensity decay within its intermediate range can be well fitted with a time constant of 45 ns). The decay has also the third, slow component that can be attributed to the contribution of trapped carriers returning to the emitting Ce^{3+} with a substantial delay. The initial acceleration of the emission decay can be attributed to the excitation transfer from activator ions Ce^{3+} to matrix-building ions Tb^{3+}. The transfer rate from Ce^{3+} to Tb^{3+} is faster than the transfer in reverse direction. The asymmetry in the excitation transfer direction is probably caused either by a fast nonradiative recombination at Tb^{3+} or a fast migration of the electrons away from Ce^{3+} via Tb^{3+} subsystem after the electrons are transferred from Ce^{3+} to Tb^{3+}. Thus, the excitation transfer results in the reduction of the population of the emitting levels $5d_1$ of Ce^{3+} acting

in parallel with the predominantly radiative recombination at Ce^{3+}. The rate of the Ce^{3+} to Tb^{3+} excitation transfer strongly depends on the distance between the ions. Thus, the transfer is efficient for the Ce^{3+} ions having Tb^{3+} in the closest proximity. The transfer rate to further Tb^{3+} is smaller than the recombination rate at Ce^{3+}, so the emission decay in its intermediate part proceeds at the rate of recombination at individual Ce^{3+}. This interpretation is also in consistence with the observation (see Fig. 3) that the fast decay component is more pronounced in the sample with the highest Tb content resulting in a higher number of the closest Ce^{3+}–Tb^{3+} pairs. The three decay components are also present at the excitation of many electron-hole pairs generated by high-energy electrons in the entire volume of the scintillator in CL experiments (see Fig. 5(d)). This is an indication that the excitation transfer from Ce^{3+} ions to the closest Tb^{3+} is the dominant mechanism accelerating the emission decay of $Tb_xGd_{3-x}Al_5O_{12}$:Ce operating as a scintillator. Our PL study shows that the Ce-Tb transfer for electrons from the second excited level $5d_2$ is more efficient than that from the lowest excited level $5d_1$.

Terbium ions also exhibit certain emission as narrow bands corresponding to optical transitions observed also in other media containing Tb^{3+} ions. In comparison to the Ce^{3+} emission, the Tb^{3+} emission is weak and spectrally overlaps with Ce^{3+} emission. A partial separation of the emissions at Ce^{3+} and Tb^{3+} reveals that the terbium emission has a fast, subanosecond, decay component. The fast decay combined with the small intensity (compared to the intensity of the luminescence of Ce^{3+} ions with a substantially lower content in the crystal than that of Tb^{3+}) evidences that the origin of this fast decay component is nonradiative recombination. Therefore, as a result of the two effects, the faster excitation transfer from Ce^{3+} to Tb^{3+} than vice versa and the strong influence of nonradiative recombination for excitations at Tb^{3+}, the incorporation of terbium in scintillator $Tb_xGd_{3-x}Al_5O_{12}$:Ce accelerates the luminescence decay but at the expense of the luminescence efficiency. Introduction of Tb up to $x = 1.3$ decreases the characteristic time of luminescence decay by 1/e to 40 ns and still exhibits the internal quantum efficiency of 30%. The further increase in Tb content results in a drastic decrease of the quantum efficiency.

Increase in Tb content in the garnet host is favorable for energy transfer via the Tb sublattice and enhances the influence of nonradiative recombination of the excitations at Tb^{3+} ions. As a result, the Tb^{3+} emission observed at Tb content $x = 1.3$ can hardly be traced in the luminescence spectra at $x = 1.5$ (see Fig. 4(b) and Fig. 5(a) for PL and CL spectra, respectively). A similar effect

has been observed in $Tb_xGd_{3-x}Al_5O_{12}$:Ce before [31] and interpreted by the dependence of excitation transfer efficiency on Tb content.

5. Conclusions

Scanning electron microscopy and cathodoluminescence images show that liquid phase epitaxy (LPE) growth from a supercooled melt solution based on $PbO-B_2O_3$ flux placed in Pt crucible enables the fabrication of thin single crystalline films of Gd- and Tb-containing garnet compounds of high structural homogeneity. Photoluminescence and cathodoluminescence spectroscopy of Ce-activated $Tb_xGd_{3-x}Al_5O_{12}$ with different Tb content *x* showed that the introduction of terbium into the garnet lattice accelerates the decay of the luminescence of activator ion Ce^{3+} due to the electron transfer from the activator ions Ce^{3+} to the closest lattice-building Tb^{3+} ions. The excitations at Tb^{3+} provide prompt photons in subnanosecond domain, but majority of the excitations at Tb^{3+} recombine nonradiatively. The internal quantum efficiency for $Tb_xGd_{3-x}Al_5O_{12}$:Ce with *x* up to 1.3 is at the level of 30%, whereas the luminescence 1/e decay time is 40 ns. The efficiency sharply drops at the further increase in Ga content.

Acknowledgements

This research has been carried out in the framework of Crystal Clear Collaboration at CERN and financially supported by the Lithuanian Research Council via project No S-CERN-24-7 and by the Polish National Scientific Centre (NCN) in the frame of Opus 24 No 2022/47/I/ST8/02600 project.

References

(Duplicates will be removed at the final formatting)

[1] P. Dorenbos, Fundamental limitations in the performance of Ce3+, Pr3+, and Eu2+ activated scintillators, IEEE Trans. Nucl. Sci. 2010, 57, 1162-1167.
[2] M. Fasoli, A. Vedda, M. Nikl, C. Jiang, B. P. Uberuaga, D. A. Andersson, K. J. McClellan and C. R. Stanek, Band-gap engineering for removing shallow traps in rare-earth Lu3Al5O12 garnet scintillators using Ga3+ doping, Phys. Rev. B, 84, 081102 (2011).
[3] K. Kamada, T. Endo, K. Tsutumi, T. Yanagida, Y. Fujimoto, A. Fukabori,
A. Yoshikawa, J. Pejchal, M. Nikl, Cryst. Growth Des. 11 (2011) 4484–4490.
[4] K. Kamada, T. Yanagida, J. Pejchal, M. Nikl, T. Endo, K. Tsutumi, Y. Fujimoto,
A. Fukabori, A. Yoshikawa, J. Phys. D: Appl. Phys. 44 (2011) 505104;

[5] K. Kamada, T. Yanagida, J. Pejchal, M. Nikl, T. Endo, K. Tsutumi, Y. Fujimoto, A. Fukabori, A. Yoshikawa, IEEE Transact. Nucl. Sci. 59 (2012) 2112–2115.

[6] K. Kamada, S. Kurosawa, P. Prusa, M. Nikl, V.V. Kochurikhin, T. Endo, K. Tsutumi, H. Sato, Y. Yokota, K. Sugiyama, A. Yoshikawa, Cz grown 2-in. size Ce:Gd3(Al,Ga) 5O12 single crystal; relationship between Al, Ga site occupancy and scintillation properties, Opt. Mater. 36 (2014) 1942–1945

[7] S. Blahuta, A. Bessiere, B. Viana, P. Dorenbos, V. Ouspenski, Evidence and consequences of Ce4+ in LYSO:Ce,Ca and LYSO:Ce,Mg single crystals for medical imaging applications, IEEE Trans. Nucl. Sci., 60, 3134-3141 (2013).

[8] M. Nikl, K. Kamada, V. Babin, J. Pejchal, K. Pilarova, E. Mihokova, A. Beitlerova, K. Bartosiewicz, S. Kurosawa, A. Yoshikawa, Defect engineering in Ce-doped aluminum garnet single crystal scintillators Cryst. Growth Des., 14, 4827-4833 (2014).

[9] M. Korzhik, G. Tamulaitis, A. Vasil'ev, Physics of Fast Processes in Scintillators, Springer, 262 pages, 2020.

[10] M. Korzhik, V. Retivov, V. Dubov, V. Ivanov, I. Komendo, D. Lelekova, P. Karpyuk, V. Mechinsky, A. Postupaeva, V. Smyslova, V. Shlegel, I. Shpinkov, A. Vasil'ev, Compositional disordering: Nanoscale engineering of advanced crystalline scintillation materials, J. Appl. Phys. 137, 020701 (2025).

[11] M.M. Kuklja, Defects in yttrium aluminium perovskite and garnet crystals: atomistic study, J. Phys. Condens. Matter 12 (2000) 2953–2967.

[12] Yu. Zorenko, A. Voloshinovskii, V. Savchyn, T. Voznyak, M. Nikl, K. Nejezchleb, V. Mikhailin, V. Kolobanov, D. Spassky, Exciton and antisite defect-related luminescence in $Lu_3Al_5O_{12}$ and $Y_3Al_5O_{12}$ garnets, Phys. Status Solidi B 244 (2007) 2180–2189.

[13] Yu. Zorenko, V. Gorbenko, I. Konstankevych, A. Voloshinovskii, G. Stryganyuk, V. Mikhailin, V. Kolobanov, D. Spassky, Single-crystalline films of Ce-doped YAG and LuAG phosphors: advantages over bulk crystals analogues, J. Lumin. 114 (2005) 85–94.

[14] Y. Talochka, S. Nargelas, Ž. Podlipskas, M. Kucera, Z. Lucenicova, G. Tamulaitis, Acceleration of emission decay in Ce-doped Gd-containing garnets by aliovalent codoping due to blocking excitation transfer via gadolinium subsystem, Radiation Physics and Chemistry, 218, 111589 (2024).

[15] A.A. Setlur, J.J. Shiang, and C.J. Vess, Transition from Long-Range to Short-Range Energy Transfer through Donor Migration in Garnet Hosts, J. Phys. Chem. C, 115, 3475-3480 (2011).

[16] K. Bartosiewicz, V. Babin, J.A. Mares, A. Beitlerova, Yu. Zorenko, A. Iskaliyeva, V. Gorbenko, Z. Bryknar, M. Nikl, Luminescence and energy transfer processes in Ce^{3+} activated $(Gd,Tb)_3Al_5O_{12}$ single crystalline films, J. Lumin. **188**, 60-66 (2017).

[17] R. Turos-Matysiak, W. Gryk, M. Grinberg, Y.S. Lin, Radiat. Meas. 42 (2007) 755.

[18] J.M. Ogieglo, A. Zych, K.V. Ivanovskikh, T. Justel, C.R. Ronda, A. Meijerink, Luminescence and Energy Transfer in $Lu_3Al_5O_{12}$ Scintillators Co-Doped with Ce^{3+} and Tb^{3+}, J. Phys. Chem. A 116 (2012) 8464.

[19] M. Zhuravleva, K. Yang, M. Spurrier-Koschan, P. Szupryczynski, A. Yoshikawa, C.L. Melcher, J. Cryst. Growth 312 (2010) 1244.

[20] A. Markovskyi, V. Gorbenko, T. Zorenko, Karol Bartosiewicz, A. Fedorov, and Y. Zorenko, Development of $Tb_{1.5}Gd_{1.5}Al_5O_{12}$:Ce Single-Crystalline Film Converters for WLED Using a Liquid Phase Epitaxy Growth Method, Crystals, 12,1814 (2022).- dublicate

[21] Zorenko, Y.; Gorbenko, V.; Zorenko, T.; Paprocki, K.; Bilski, P.; Twardak, A.; Voznyak, T.; Sidletskiy, O.; Gerasimov, Y.; Gryniov, B., et al. Composition Engineering of Single Crystalline Films Based on the Multicomponent Garnet Compounds. Opt. Mater. (Amst.) 2016, 61, 3–10.

[22] Gorbenko, V.; Zorenko, T.; Witkiewicz, S.; Paprocki, K.; Sidletskiy, O.; Fedorov, A.; Bilski, P.; Twardak, A.; Zorenko, Y. LPE Growth of Single Crystalline Film Scintillators Based on Ce3+ Doped Tb3□xGdxAl5□yGayO12 Mixed Garnets. Crystals 2017, 7, 262 .

[23] S. Leyre, E. Coutino-Gonzalez, J.J. Joos, J. Ryckaert, Y. Meuret, D. Poelman, P.F. Smet, G. Durinck, J. Hofkens, G. Deconinck, P. Hanselaer, Absolute determination of photoluminescence quantum efficiency using an integrating sphere setup, Rev. Sci. Instrum. 85 (2014) 123115.

[24] V. Khanin, A.-M. van Dongen, D. Buettner, C. Ronda, and P. A. Rodnyi, Scintillator-Oriented Investigation of Y3Al5O12:Ce,Tb Powders, ECS J. Solid State Sci. Technol. 4 R128 (2015).

[25] A. Markovskyi, V. Gorbenko, T. Zorenko, Karol Bartosiewicz, A. Fedorov, and Y. Zorenko, Development of $Tb_{1.5}Gd_{1.5}Al_5O_{12}$:Ce Single-Crystalline Film Converters for WLED Using a Liquid Phase Epitaxy Growth Method, Crystals, 12,1814 (2022).- dublicate

[26] S. Nargelas, Y. Talochka, A. Vaitkevičius, G. Dosovitskiy, O. Buzanov, A. Vasil'ev, T. Malinauskas, M. Korzhik, G. Tamulaitis, Influence of matrix composition and its fluctuations on excitation relaxation and emission spectrum of Ce ions in (Gd*x* Y1-*x*)3Al2Ga3O12: Ce scintillators, J. Lumin. **242**, 118590, (2022).

[27] Bartosiewiwicz

[28] K. Szyszka, M. Kardach, D. Szymański, R. J. Wiglusz, Synthesis, characterization, and temperature-dependent luminescence of Tb^{3+}-activated and self-activated $Sr_{10}(PO_4)_6Cl_2$ phosphors, J. Lumin. 275, 120788 (2024).

[29] I. Gupta, D. Singh, S. Singh, P. Kumar, S. Bhagwan, V. Kumar, H. Kumar, S.K. Chhikara, Crystallographic, morphological and photoluminescent investigations of Tb3+-doped YAlO3 perovskites for lighting applications, Luminescence, 38 (2023) 585-599.

[30] I. Gupta, D. Singh, S. Singh, P. Kumar, S. Bhagwan, V. Kumar, H. Kumar, S.K. Chhikara, Crystallographic, morphological and photoluminescent investigations of Tb3+-doped YAlO3 perovskites for lighting applications, Luminescence, 38 (2023) 585-599.

[31] Bartosiewicz